Applied Catalysis B: Environmental 324 (2023) 122252

Contents lists available at ScienceDirect

Applied Catalysis B: Environmental

journal homepage: www.elsevier.com/locate/apcatb

Highly active and selective H_2O_2 electrosynthesis in O-rich ZIF-67 derived Co-N/O-C cathode for ofloxacin oxidation

Zunxing Liu [a], Dong Wang [b,*], Mengqiong Zhang [a], Hongchao Ma [a], Guowen Wang [a,*]

[a] School of Light Industry and Chemical Engineering, Dalian Polytechnic University, No. 1 Qinggongyuan, Ganjinzi District, Dalian 116034, PR China
[b] College of Marine Science-Technology and Environment, Dalian Ocean University, No. 52 Heishijiao, Shahekou District, Dalian 116023, PR China

ARTICLE INFO

Keywords:
Hydrogen peroxide
ZIF-67
Oxygen reduction reaction
Oxygen functional groups

ABSTRACT

Electrochemical production of hydrogen peroxide (H_2O_2) via 2-electron pathway is the most promising alternative to the anthraquinone process. However, designing and synthesizing electrocatalysts with high activity and high selectivity remains a challenge. Here, we evaluated a facile and efficient approach of improving the catalyst activity and selectivity by introducing O functional group into Co-N-C catalysts, which pyrolyzed at different temperatures. Our analyses showed that the catalyst activity and selectivity were related with the oxygen-containing functional groups and the pyrolysis temperature. H-cell test produced a H_2O_2 output of 2170 ppm within 6 h, which met the in-situ degradation of antibiotics (Ofloxacin), offering a reliable on-site environmental treatment option.

1. Introduction

Hydrogen peroxide (H_2O_2) is one of the most used chemical in various processes such as chemical, paper or pollutant degradation, and has shown great potential in environmental remediation due to its excellent oxidizing properties and environment-friendly nature. Therefore, there is a huge demand for H_2O_2, which has led to an urgent need for efficient, cheap, and environmentally friendly synthesis technologies [1–4]. Currently, industrial synthesis of H_2O_2 is based on anthraquinone technology, a process that involves multiple reaction steps. Besides, the anthraquinone technology requires a large infrastructure, and generates many toxic and harmful by-products, contrary to the global quest for green chemistry [5]. Although direct reaction of hydrogen and oxygen in the presence of a catalyst is an attractive pathway in producing H_2O_2 ($H_2+O_2=H_2O_2$) [6], it has potential explosion hazards, which compromises the industrial production of H_2O_2 [7]. Another alternative route is direct synthesis of H_2O_2 by electrochemical methods (via the $2e^-$ pathway of ORR). Unlike the anthraquinone method, the electrochemical synthesis of H_2O_2 yields water as the only by-product, which converges with the green chemistry aim [8–10]. Despite the advantages of electrochemical synthesis of H_2O_2, the oxygen reduction reaction is kinetically slow. More importantly, it's quite different ORR pathway including $4e^-$ and $2e^-$ for electrochemical catalyst. In addition, the ORR reaction requires catalysts to accelerate the process and reduce the overpotential of ORR. Currently, precious metals [11]and their alloys such as (Pd-Au [12], Pt-Hg [13], Au-Pt [14], Pd-Hg [15]) are the best available catalysts due to their high catalytic activity and selectivity. However, they are associated with high costs, thus limiting their commercial application [16]. Therefore, development of efficient and durable catalyst materials in electrochemical production of H_2O_2 without inclusion of precious metals is key in achieving commercial needs.

MOF materials have received a lot of attention in catalysis due to their unique properties such as high stability, tunable pore size structure, simple heteroatom doping, and diverse composition. In addition, it has been shown that many of the MOF materials (ZIF-67, ZIF-8, etc.) have high catalytic activity in ORR, providing an opportunity for reliable and renewable electrocatalysts after carbonization [17–19]. Although the MOF-based catalysts have high catalytic activity in ORR, they prefer the $4e^-$ process to produce water rather than the $2e^-$ process to produce H_2O_2. Previous studies have evaluated how to improve the selectivity and activity of catalysts, including heteroatom doping (N [20,21], B [22,23], S [24,25], O [8,26–28], F [29]), which has been considered and explored as an effective way to improve the selectivity of ORR. The introduction of oxygen-containing functional groups gives carbon materials hydrophilicity, high electrical conductivity and electroactivity, which accelerates migration of oxygen to the electrocatalyst surface in the liquid phase [30]. Cui Yi [8] et al. demonstrated that both activity and selectivity in the ORR reaction are positively correlated

* Corresponding authors.
E-mail addresses: wangdong@dlou.edu.cn (D. Wang), guowen@dlpu.edu.cn, wanggw@dlpu.edu.cn (G. Wang).

https://doi.org/10.1016/j.apcatb.2022.122252
Received 3 April 2022; Received in revised form 8 September 2022; Accepted 30 November 2022
Available online 5 December 2022

with the oxygen content of the catalyst, while carbon atoms adjacent to oxygen functional groups (-COOH and C-O-C) are active centers for the oxygen reduction reaction via the two-electron pathway. In addition, Wu [31] et al. showed that the charring temperature of the MOF materials affects the final valence state of Co coordinated with N in the catalyst. This strong coordination between Co and N leads to the transfer of electrons from the Co to N. The electron-absorbing property of N leads to a decrease in the electron density of the Co center, which significantly changes the electron structure of the adjacent carbon atoms which then improves the ORR activity as well as other similar study [32]. To investigate the effect of this change on the ORR $2e^-$ process, we performed pyrolysis of the precursors at different temperatures.

We then prepared highly active and selective hydrogen peroxide-producing electrocatalysts by adding oxygen-containing functional groups to the surface of the Co-N-C catalysts, pyrolyzed with ZIF-67 precursors. The catalysts, with the additional oxygen-containing functional groups (Co-N/O-C-x, x = 700, 800, 900 °C) had higher $2e^-$ selectivity compared to those without. In addition, as predicted, the pyrolysis temperature influenced the catalyst activity to some extent, and the catalyst with the highest pyrolysis temperature (Co-N/O(R)-C-900) exhibited the highest catalytic activity. Besides, the H-cell tests demonstrated good durability of the catalyst, and the generation of H_2O_2 satisfied the in-situ degradation of pollutants, which might be a novel strategy for treatment of wastewater.

2. Materials and methods

2.1. Synthesis of Co-N/O(R)-C-x

We synthesized the Co-N/O(R)-C-x catalyst as shown in Fig. 1a. To synthesize ZIF-67, we dissolved $Co(NO_3)_2$-6 H_2O (1 g) in 50 mL of methanol, and then added 2.5 g of 2-methylimidazole methanol solution (80 mL). The mixture was stirred at room temperature for 30 min, sealed, and then left at room temperature for 12 h. The formed violet crystals were separated by centrifugation (5000 rpm), washed 3 times in methanol, and then dried overnight at 60 °C under vacuum. 600 mg of ZIF-67 was placed in a quartz boat, which was placed at the center of a furnace equipped with horizontal quartz tubes. Under nitrogen atmosphere, it was pyrolyzed at a heating rate of 5–700 °C, 800 °C, and 900 °C for 2 h, and then cooled to room temperature. The resulting catalysts were treated with an oxidizing acid solution to remove cobalt nanoparticles and modify the oxygen-containing functional groups. 300 mg of Co-N-C-x (x = 700, 800, 900) was added to 250 mL of aqueous nitric acid solution (10.0 $molL^{-1}$) and then sonicated for 5 min to form a homogeneous suspension. Thereafter, the suspension was heated to 75 °C and continuously stirred for 48 h for acid etching and oxidation. After cooling to room temperature, the suspension was filtered and washed 3 times with deionized water and ethanol. It was then dried in a vacuum oven at 80 °C. As a control, the catalyst was subjected to acid leaching using a non-oxidizing acid (10 $molL^{-1}$ HCl).

2.2. Hydrogen peroxide in H-cell test

To quantify the concentration of H_2O_2, we performed electrochemical ORR in a H-cell, with a N115 membrane as the septum. The volume of both the three-well chamber (working electrode, with SCE as reference electrode) and the two-well chamber (graphite rod as counter electrode) of the cell was 50 mL, and each chamber was filled with 40 mL of 0.1 M KOH electrolyte. The same catalyst ink was sprayed onto Teflon-treated carbon paper (1 cm × 1 cm, Toray, TGPH090) with a gun, at a catalyst loading of ~1 mg cm^{-2}. To ensure saturation of the oxygen concentration within the electrolyte, the electrolyte in the cathode chamber was bubbled with pure O_2 gas. The polarization curves were obtained by linear scanning voltammetry (10 mV/s^{-1}). Since the device is more likely to operate at a constant potential or current, we tested the long-term stability of the cobalt monatomic catalyst in an H-type device (0.5 V by chrono-current method). In addition, we determined the durability of the catalyst using chrono-potential method (I = 50 mA).

2.3. Electrochemical degradation via hetero-electro-fenton process

Degradation and mineralization of contaminants was carried out in a single cell with a three-electrode system. A platinum electrode, a saturated calomel electrode and carbon paper (Toray, TGPH090) were used as counter a electrode, reference electrode and working electrode, respectively. Then a 2 × 2 cm^2 sheet of carbon paper was evenly coated with the catalyst ink to an ink loading of 1.5 mg cm^{-2}. Electrocatalytic degradation experiments were carried out with 5 mg L^{-1} ofloxacin in O_2-saturated 0.1 M Na_2SO_4 solution at − 1.3 V (vs. SCE). Current-time (i-t) was recorded during the reaction. The pH of the electrolyte was adjusted with 0.1 M H_2SO_4 or NaOH. To determine the degradation performance of the catalyst, ofloxacin concentration was determined by UV–vis spectrophotometer at a wavelength of 288 nm (Fig. S3).

3. Results and discussion

3.1. Characterization of the structure and morphology

The basic characteristics of the catalyst precursors are as shown in Fig. 1. Compared to the standard sample, the diffraction peaks of the XRD pattern of the ZIF-67 were in perfect agreement with the diffraction peak positions (Fig. S1), which showed standard crystallinity without any detectable by-products. To confirm the addition of oxygen-containing functional groups, we performed Fourier transform infrared (FTIR) spectroscopy (Fig. 1b). 3438 cm^{-1}, 1720 cm^{-1}, 1167 cm^{-1} for O-H, C═O, and C-O bonds, respectively, as well as the catalyst that underwent HNO_3 treatment (Co-N/O-C-800) showed larger peaks, compared to the catalyst treated with the control (HCl) (Co-N/R-C-900, Co-N/R-C-800), which indicated successful addition of oxygen-containing functional groups in the catalysts [8]. The XRD patterns (Fig. S4) of the catalysts after pyrolysis acid leaching showed an increasing degree of charring with increasing pyrolysis temperature. The data showed that the degree of charring can only be influenced by the pyrolysis temperature while the acid leaching treatment did not affect the crystal morphology. The characteristic peak at 2θ= 26.3° in the XRD pattern corresponded to the (002) plane of graphitic carbon, which mirrored the conversion of amorphous carbon to graphitic carbon during the pyrolysis. The characteristic peak at 2θ= 44° corresponded to the (111) plane of face-centered cubic Co.

Analysis of oxidation degree of the Co-N/O(R)-C-800 was carried out using X-ray photoelectron spectroscopy (Fig. 1d). The presence of the intensive O1s peak in Co-N/O-C-800 indicated that O-containing groups occurred after etching treatment by HNO_3. On the other hand, scanning electron microscopy (SEM) showed that the Co-N/O(R)-C-x obtained after high-temperature pyrolysis carbonization inherited the overall polyhedral morphology of the precursor ZIF-67 and exhibited a more regular rhombic orthododecahedral structure (Fig. 1e and f). With increase in the pyrolysis temperature, there was collapse of rhombic dodecahedral structure, which is a normal phenomenon during high-temperature pyrolysis of ZIF-67 [33]. EDS-mapping showed successful addition of oxygen-containing functional groups, which is consistent with the FTIR results (Fig. 1g and h). Nitrogen isothermal adsorption and desorption curves showed that the specific surface area of the catalyst decreased with increasing pyrolysis temperature(367 m^2g^{-1} (700 °C) > 306 m^2g^{-1} (800 °C) > 244 m^2g^{-1} (900 °C))because of the collapse of carbon structure due to the increase in the carbonization temperature [34] (Fig. S5).

3.2. Electrocatalytic activity and stability of Co-N/O(R)-C-x

We tested ORR performance of the Co-N/O(R)-C-x (Fig. 2a),

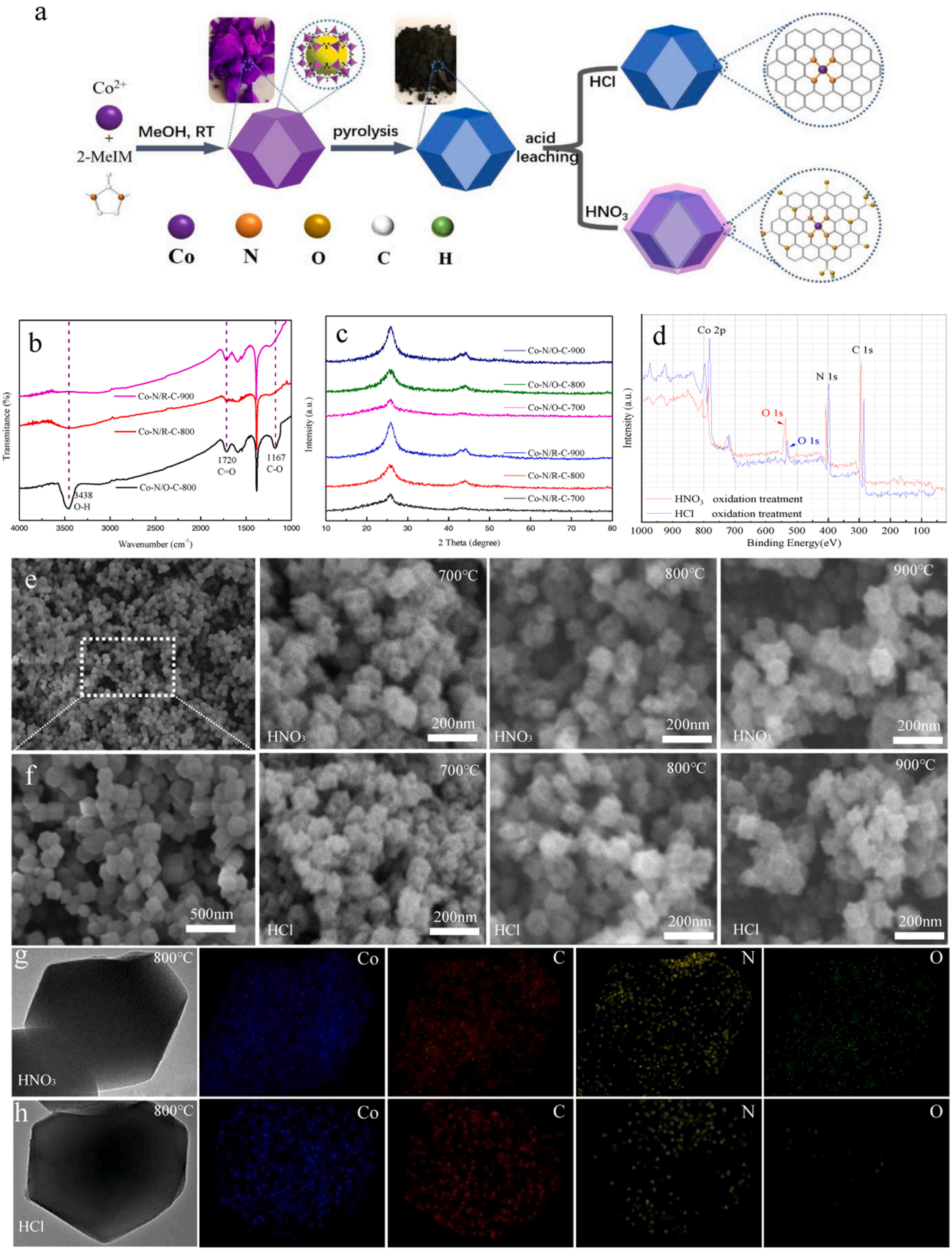

Fig. 1. (a) Schematic illustration of the synthesis process for Co-N/O(R)-C-x (x = 700 °C, 800 °C, 900 °C). (b) FTIR spectra of Co-N/R-C-900、Co-N/R-C-800、and Co-N/O-C-800. (c) X-ray pattern of Co-N/O(R)-C-x samples. (d) Co 2p and O 1 s XPS spectra of the Co-N/R-C-800 and Co-N/O-C-800 treated with HCl and HNO_3, respectively. (e) and (f) SEM image of samples prepared under different temperature and etching conditions. bottom: TEM and EDS-mapping of Co-N/O-C-800 catalyst (g), apparent O signals accumulating in green and Co-N/R-C-800 (h) catalyst (less cobalt ions are due to the masking effect of chloride ions).

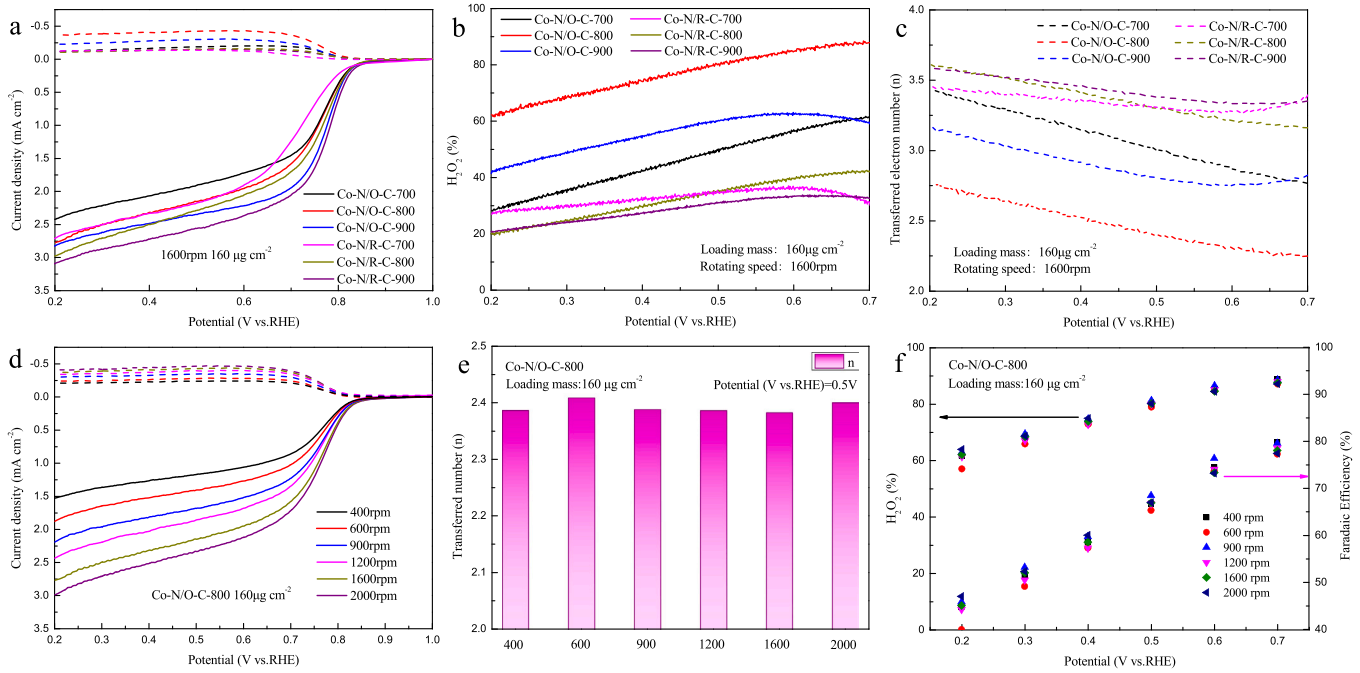

Fig. 2. (a) RRDE test curve, (b) Hydrogen peroxide yield (H_2O_2 %), (c) transferred electron number (n) of catalyst Co-N/O(R)-C-x (x = 700, 800, or 900 ℃). (d) RRDE curve with different speeding, (e) transferred electron number (n), (f) Hydrogen peroxide yield (H_2O_2 %) (left) and faradaic efficiency (%) (right) of Co-N/O-C-800.

especially in the H_2O_2 production by the $2e^-$ pathway. According to our CV test results (Fig. S6), Co-N/R-C-900 had the highest disk current density (I_d=3.1 mA cm^{-2}) and half-wave potential ($E_{1/2}$ =0.76 V). Unfortunately, however, the ring current density (I_r) of Co-N/R-C-900 was low. The oxidized Co-N/O-C-x series catalysts exhibited a pleasant ring current density compared to the Co-N/R-C-x. In addition, the highest disk current density (I_d=2.95 mA cm^{-2}) for Co-N/R-C-800 and Co-N/O-C-900 exhibited the highest ring current density. To compare the production performance of the Co-N/O(R)-C-x series catalysts, we calculated the H_2O_2 yield (H_2O_2 %) (Fig. 2b) and the number of transferred electrons (n) (Fig. 2c). The data showed that the H_2O_2 yield in the Co-N/O(R)-C-x series catalysts were Co-N/O-C-800 (74.5 %) > Co-N/O -C-900 (54.6 %) > Co-N/O-C-700 (42.3 %) > Co-N/R-C-700 (32.4 %) > Co-N/R-C-800 (30.0 %) > Co-N/R-C-900 (27.3 %), while the number of electrons transferred (n) for the Co-N/O(R)-C-x series catalysts were Co-N/O-C-800 (2.40) < Co-N/O-C-900 (2.91) < Co-N/O-C-700 (3.14) < Co-N/R-C-700 (3.34) < Co-N/R-C-800 (3.41) < Co-N/R-C-900 (3.45). Thus, the oxidized catalysts improved the H_2O_2 yields, which demonstrates that the presence of oxygen-containing functional groups favors the $2e^-$ process of ORR [3]. In addition, the catalysts we prepared also showed good selectivity and reactivity (Table S1 and S2). We then calculated the Faraday efficiency (FE %) of the catalysts, and in agreement with the above results, Co-N/O-C-800 exhibited optimal catalyst activity and selectivity among the oxidized Co-N/O-C-x series catalysts (Fig. S7). These findings were associated with the pyrolysis temperature. If the heating temperature is too low, the cobalt and nitrogen sources do not react to form the active center [35]. In addition, the carbonization could not be completed, resulting in poor electrical conductivity and structural instability. However, heat treatment at higher temperatures often lead to the loss of nitrogen due to the collapse of the carbon structure, which makes the catalyst $2e^-$ pathway less selective for H_2O_2 production [31,36].

Based on the excellent H_2O_2 production by the Co-N/O-C-800 catalyst, we measured the LSV curves at different rotational speeds using a ring-disk electrode (RRDE) in an oxygen-saturated 0.1 M KOH solution. The starting potential (Eon) of the catalyst was the same, while the limiting current density of the ring current (I_r) and disk current (I_d) increased with the increase of the rotational speed (Fig. 2d). This phenomenon was caused by decrease in the polarization of the solution with the increase of the rotational speed of the rotating ring-disk electrode. We further calculated the number of electrons (n) (Fig. 2e) transferred from the catalyst at different rotational speeds at a voltage of 0.5 V (vs. RHE). The findings showed that the number of electrons transferred from the catalyst at different rotational speeds was the same. Similarly, the H_2O_2 % and Faraday efficiency (FE %) of the catalysts at different rotational speeds at the same voltage were the same (Fig. 2f).

To define the effect of catalyst loading on catalyst activity and selectivity, we measured the LSV curves at different loading levels using a ring-disk electrode (RRDE) in an oxygen-saturated 0.1 M KOH solution (Fig. 3a). The ring and disk currents increased gradually with increased catalyst loading from 80 μg cm^{-2}, 110 μg cm^{-2}, and 160 μg cm^{-2}, while the ring current density decreased significantly when the catalyst loading was 220 μg cm^{-2}. However, the disk current density reached the maximum. To assess the effect of loading on the selectivity of H_2O_2 production, we calculated H_2O_2 % (Fig. 3b), the number of electrons transferred (n) (Fig. 3c), and FE % (Fig. 3d). The selectivity of the $2e^-$ process was indeed favored at lower loadings. This could be because the possibility and time of peroxide disproportionation and/or electroreduction decreased along the diffusion path (from the electrode to the electrolyte) with reduction of the catalyst loading (thinner electrode layer) [37]. Therefore, reducing the catalyst loading can reduce the residence time of H_2O_2 on the catalyst surface, thus reducing the amount of H_2O_2 reduced to H_2O, thus improving the selectivity of H_2O_2 [17,38]. To determine the peroxide reduction reaction (PRR) within the catalytic layer, we employed similar method to determine the electrochemical activity of Co-N/O(R)-C-x catalysts for H_2O_2 reduction in an electrolyte saturated with N_2 at 3 mM H_2O_2 + 0.1 M KOH (Fig. 3e). The stronger PRR of the non-oxidizing acid-treated catalysts compared to the Co-N/O-C-x series catalysts maybe because the catalytic multi-electron ORR required different metal single-atom sites, which may proceed through direct $4e^-$ channels or indirect $2e^-$ channels involving H_2O_2 intermediates. Further electroreduction of H_2O_2 to H_2O at the active center is detrimental to the efficient production of H_2O_2, and therefore PRR ($H_2O_2 \rightarrow H_2O$) catalysis should be inhibited [39]. In addition, our

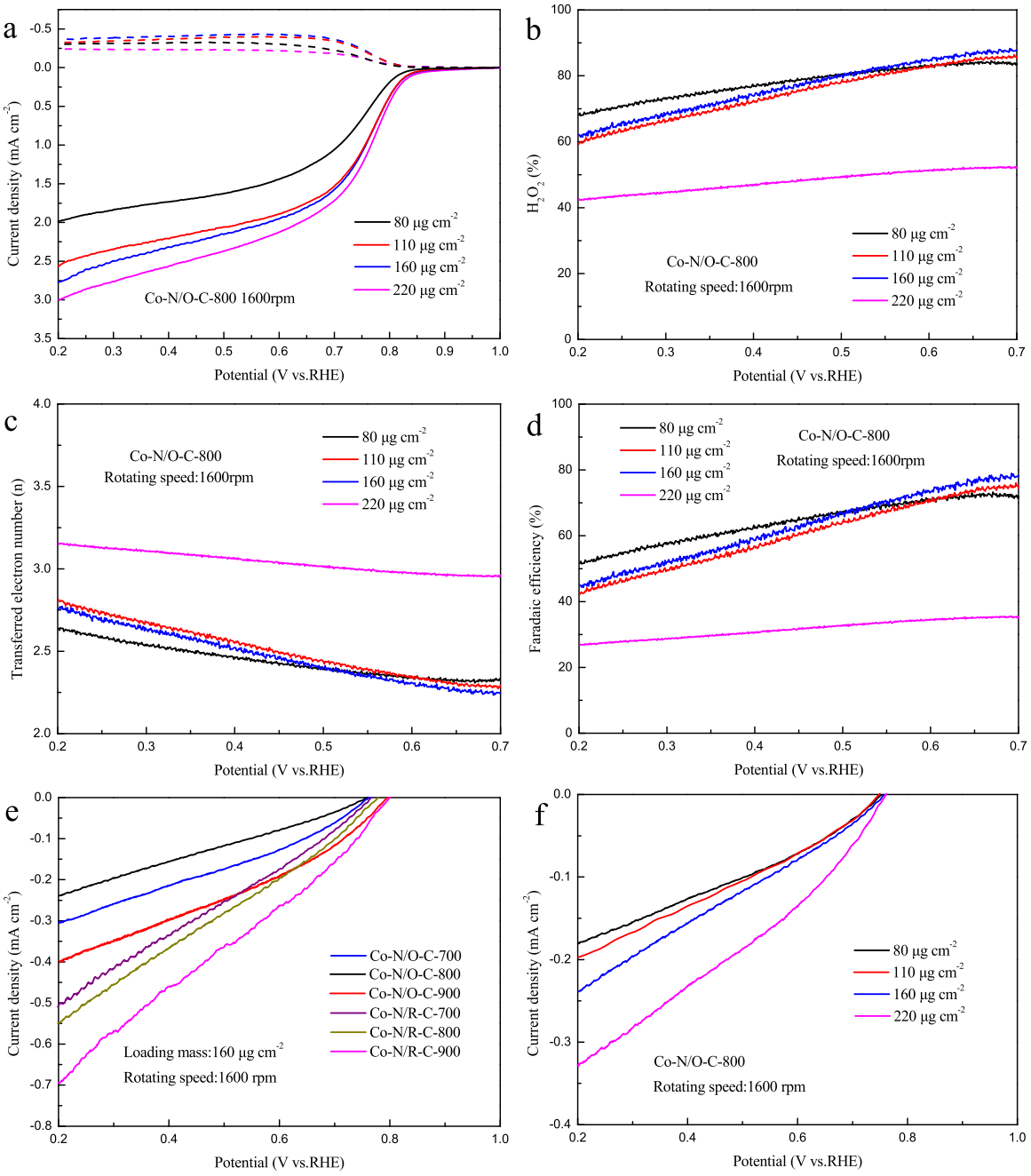

Fig. 3. (a) RRDE curve with different loadings, (b) Hydrogen peroxide yield (H_2O_2 %), (c) transferred electron number (n), (d) faradaic efficiency (%) of Co-N/O-C-800. (e) Peroxide reduction reaction (PRR) curves of Co-N/O(R)-C-x(x = 700, 800, 900 ℃), (f) PRR curves of Co-N/O-C-800 with different loading (Containing 3.5 mM H_2O_2).

PRR tests with different catalyst loadings confirmed the above observation (Fig. 3f).

3.3. *Performance of the Electrocatalytic H_2O_2 Synthesis*

Also, we compare the predicted COOH group versus C═O and OH, which was intended for revealing the effect of oxygen functional groups in Co-N/O-C-800. Further analysis indicate that COOH groups mainly contribute the selectivity for H_2O_2 production but the C═O and OH groups could also contribute to active sites according to chemical titration (Fig. S8). To assess H_2O_2 production in a real life, a two-chamber H-type electrochemical cell was customized and tested (Fig. 4a). First, to determine the appropriate catalyst loading on carbon paper, the polarization curve of the catalyst was measured (Fig. 4b). The increase in catalyst loading resulted in an increase of the active sites on the electrode surface (electrode surface area of 1 cm^{-2}), which resulted in a slight positive shift in the onset potential and an increase in the current density[39]. Actual H_2O_2 production using the best performing Co-N/O-C-800 catalyst in our assembled H-cell yielded a H_2O_2 concentration of 2170 ppm after 6 h (for applications requiring dilute H_2O_2 solutions) (Fig. 4c, Fig. S1). The H_2O_2 concentration also depended on the initial volume of the electrolyte. Previously, several cell designs for the electrochemical production of H_2O_2 that use small reactors with small electrolyte volumes were proposed [40]. However, the cumulative concentration of H_2O_2 is easily reduced by further reduction of H_2O_2 to H_2O or chemical decomposition to O_2. Our results showed that the H_2O_2 molecules decomposed more readily as the initial H_2O_2 increased. A solution to this problem was to use a new type of cell, such as a flow cell,

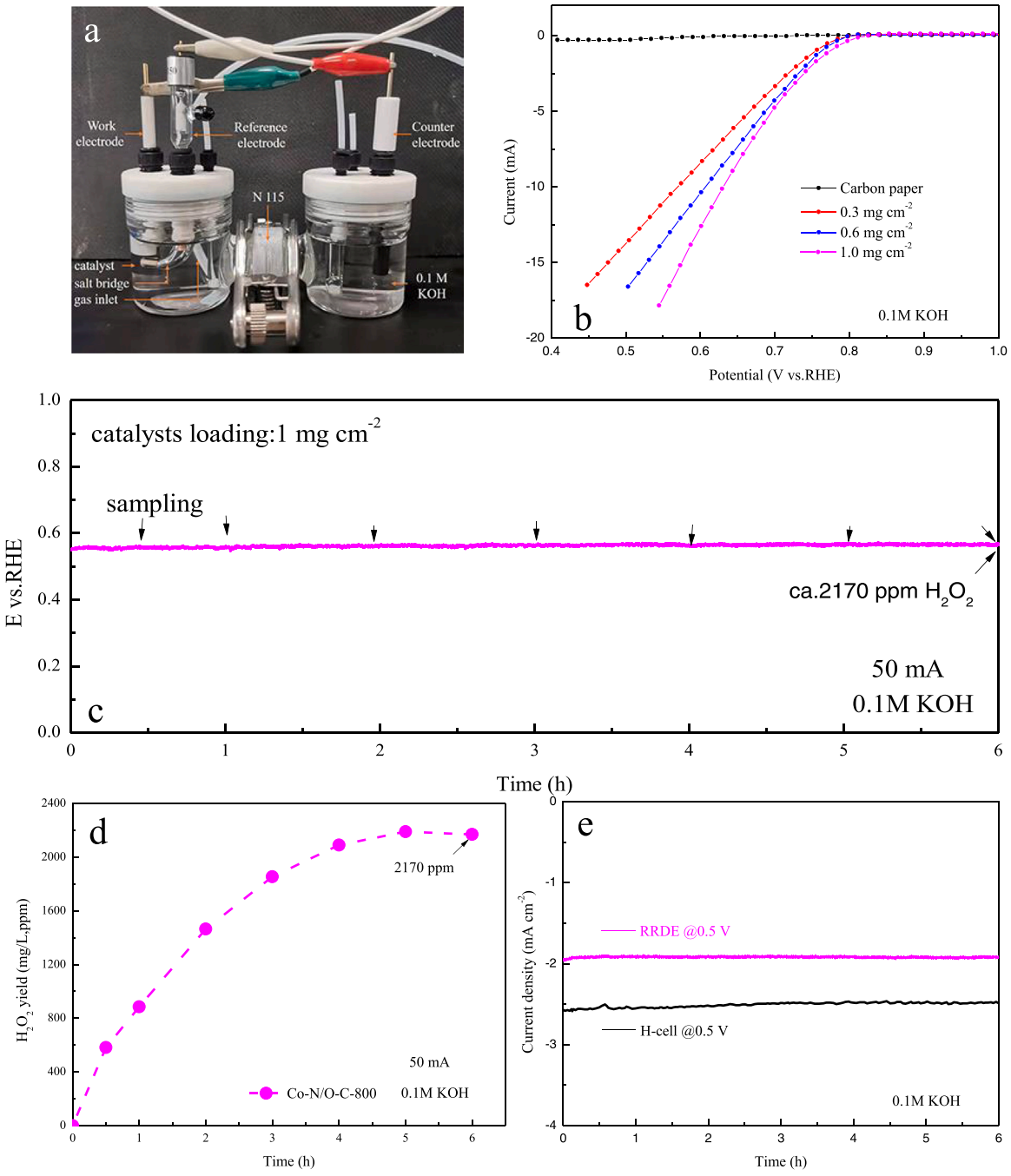

Fig. 4. (a) Custom-made electrochemical H-type cell. (b) O_2 reduction results obtained on the carbon paper electrode loaded with Co-N/O-C-800 in O_2-saturated 0.1 M KOH electrolyte. IR-corrected polarization curves as a function of catalyst loading weight. (c) V-t curve under a constant current of 50 mA of the Co-N/O-C-800 catalyst for producing H_2O_2. (The arrow indicates the sampling point, which is used to detect the accumulation of H_2O_2) (d) Accumulation of H_2O_2. (e) Chronoamperometry stability tests for Co-N/O-C-800 evaluated by RRDE and in H-cell.

which can prevent accumulation of H_2O_2 and thus improve current efficiency [17]. With further improvements in H_2O_2 storage technology, it is expected that our Co-N/O-C-800 can exhibit even higher H_2O_2 storage performance. Finally, we evaluated the electrochemical stability of Co-N/O-C-800 by timing current testing and overall electrolysis using RRDE in the custom H-cell (Fig. 4e). The results showed that both catalysts exhibited excellent durability with only a slight decrease in current density over a period of 6 h.

3.4. Electrocatalytic degradation of antibiotics

The ability of the in-situ produced H_2O_2 to degrade and mineralize refractory organic pollutants in wastewater was assessed (Fig. 5a). The hydroxyl radicals (·OH) were generated directly by the H_2O_2 dissociation or ORR pathways during the electrocatalytic reaction, and the characteristic signals with relative intensities of 1:2:2:1 were detected by electron paramagnetic resonance spectroscopy (EPR) at 60 min and 90 min using 5,5-dimethyl-1-pyrroline N-oxide (DMPO) as a self-selected trap (Fig. 5b). IPA-·OH adducts and DMPO control treatment did not have characteristic signals in the EPR spectra (Fig. 5c), thus confirming the presence of hydroxyl radicals (·OH) at 60 min and 90 min. We then selected Ofloxacin (OFL) as a representative micropollutant due to its chemical stability and persistence. Considering the high specific surface area of MOF material catalyst on the adsorption of

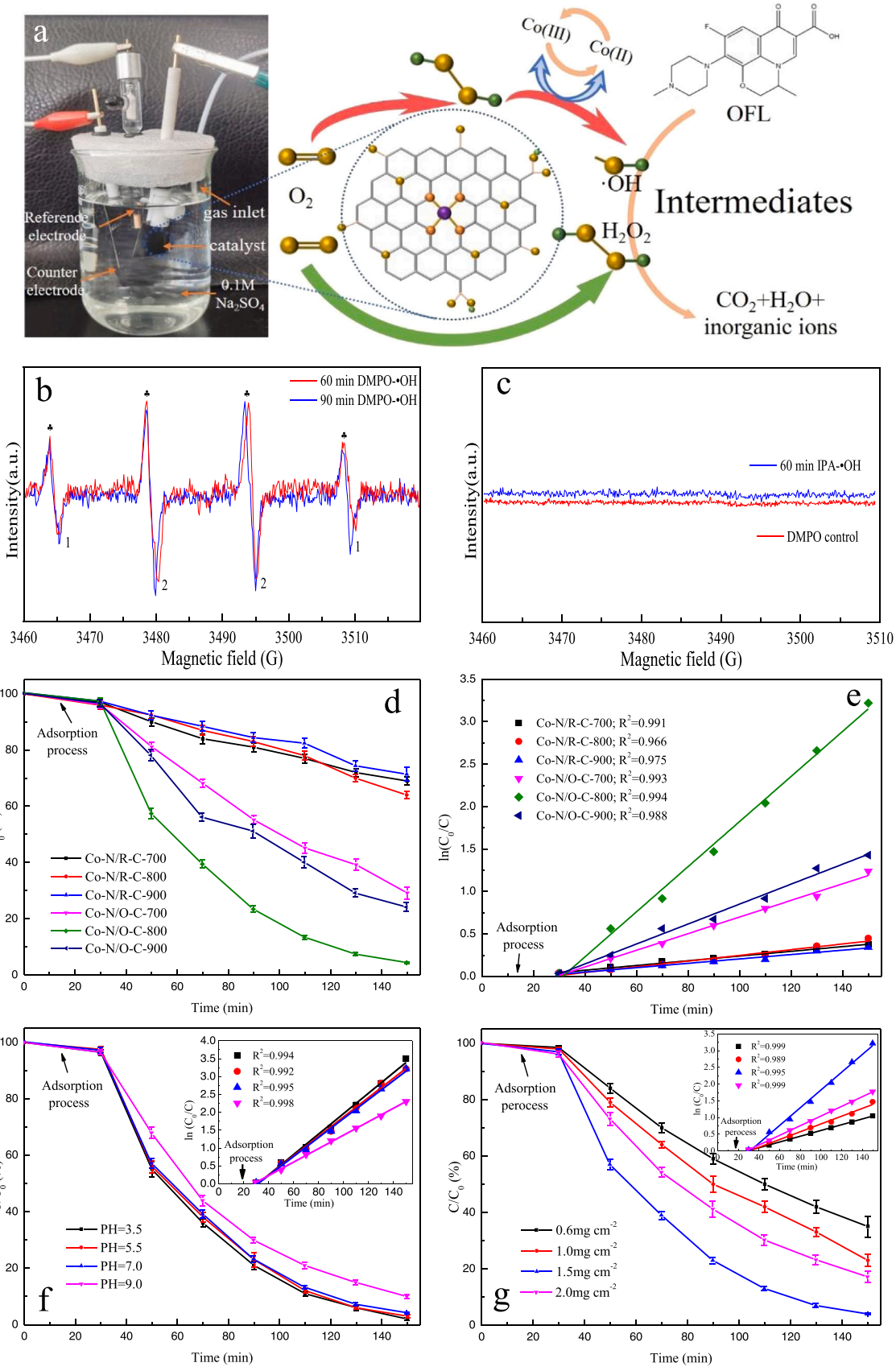

Fig. 5. (a) Schematic diagram of Co-N/O(R)-C-x cathodic degradation of ofloxacin (OFL). (b) DMPO spin trapping EPR spectra for •OH. (c) EPR spectrum of DMPO control treatment and addition of IPA inhibitor. (d) Degradation efficiency of ofloxacin (OFL) and (e) corresponding kinetic analyses. (f) Degradation efficiency of OFL at different pH values over Co-N/O-C-800 cathodes. Inset: corresponding kinetic analyses. (g) Degradation efficiency of OFL at different loading mass values over Co-N/O-C-800 cathodes. Inset: corresponding kinetic analyses.

OFL, the carbon paper coated with the catalyst (working cathode) was soaked in the solution for 30 min and then energized. The adsorption experiments revealed that the degradation rate of OFL was only about 3 %, which was attributed to the high specific volume of the catalyst. After two hours of degradation, Co-N/O-C-800 showed the highest degradation rate (96 %), under neutral conditions (Fig. 5d). Besides, maximum apparent rate constant of the catalyst was 0.0272 min^{-1} of Co-N/O-C-800, the comparative values of other catalysts was Co-N/O-C-900 (0.0123 min^{-1}) > Co-N/O-C-700 (0.0101 min^{-1}) > Co-N/R-C-800 (0.0037 min^{-1}) > Co-N/R-C-700 (0.0031 min^{-1}) > Co-N/R-C-900 (0.0028 min^{-1}) (Fig. 5e). Our data showed that the catalysts treated with surface oxidation had more excellent degradation performance, which was attributed to the excellent H_2O_2 production ability of the catalysts. In addition, we investigated the degradation performance of the catalysts with different temperature pyrolysis, and showed that the degradation ability of Co-N/O-C-900 (76 %) and Co-N/O-C-700 (71 %) was significantly weaker than that of Co-N/O-C-800. This result was consistent with the observation from the catalyst performance analysis on H_2O_2 production. On the other hand, the effect of initial pH on cathodic degradation of OFL by Co-N/O-C-800 was investigated. The degradation rates of OFL were 98 %, 97 %, 96 %, and 90 % at initial pH of 3.5, 5.5, 7.0, and 9.0, respectively (Fig. 5f). The decline in performance from acidic to alkaline solutions can be attributed to the decrease in oxidation potential of -OH from ~2.7–1.9 V [41]. The effect of different catalyst loadings on the degradation of OFL was investigated and the results demonstrated that Co-N/O-C-800 cathode had optimal degradation performance (96 %) when the catalyst loading was 1.5 mg cm^{-2}. Besides, the catalyst degradation efficiency gradually increased when the catalyst loading was 0.6 mg cm^{-2} (65 %) and 1.0 mg cm^{-2} (77 %), respectively. However, when the catalyst loading reached 2.0 mg cm^{-2} (83 %), the degradation efficiency decreased significantly, which may be because the over-thick catalytic layer reduced the ORR selectivity, resulting in a reduced H_2O_2 yield and thus affecting degradation efficiency (Fig. 5g). The degradation efficiency of antibiotics is associated with the cathodic electrolytic potential [36,42]. When the potential negatively shifts from − 1.0 V vs.SCE to − 1.5 V vs. SCE, the degradation efficiency of ofloxacin increases from 82 % to 96 %. Considering the energy saving and electrocatalytic activity, we chose the potential of − 1.3 V (Fig. S9).

4. Conclusion

In summary, fully experimental electrochemical data demonstrated that the selectivity of Co-N/O-C catalyst can be improved by 42.1 % (E = 0.4 V vs. RHE) via facile nitric acid oxidation treatment. Various oxygen functional groups such as COOH and CO are confirmed as active sites in activity and selectivity contributions for $2e^-$ ORR pathway. Looking across different pyrolysis temperatures, the Co-N/O-C-800 is determined to be the optimal catalyst for $2e^-$ ORR with the high ring current density and 74.5 % of H_2O_2 yield. Further H-cell tests confirmed efficient H_2O_2 production (2170 ppm) and excellent durability (> 6 h) of the catalysts. Then the application efficiency of the onsite electro-generated H_2O_2 was evaluated using antibiotic as model emerging contaminant. It gives satisfying results in terms of removal rate and mineralization ratio of ofloxacin. Together, our study provides new insights into efficient H_2O_2-producing catalysts, especially with respect to MOF materials, for rational design of novel catalysts in the field of environmental remediation.

CRediT authorship contribution statement

Zunxing Liu: Writing – original draft, Visualization, Formal analysis. **Dong Wang:** Writing – original draft, Validation. **Mengqiong Zhang:** Resources, Methodology. **Hongchao Ma:** Supervision, Data Curation, Investigation. **Guowen Wang:** Conceptualization, Supervision, Writing – review & editing.

Declaration of Competing Interest

The authors declare that they have no known competing financial interests or personal relationships that could have appeared to influence the work reported in this paper.

Data Availability

Data will be made available on request.

Acknowledgements

The authors greatly appreciate basic scientific research projects of colleges and universities for youths granted by The Educational Department of Liaoning Province (No. LJKQZ2021118 and No. LJKZ0707). Financial support for this work was partialy provided by youth project No. 42107505 and No. 21407017, granted by National Natural Science Foundation of China (NSFC). Guowen Wang also thank the Natural Science Foundation of Liaoning Province for forceful policy support (project NO. 2019-MS-016).

Appendix A. Supporting information

Supplementary data associated with this article can be found in the online version at doi:10.1016/j.apcatb.2022.122252.

References

[1] W.R.P. Barros, R.M. Reis, R.S. Rocha, M.R.V. Lanza, Electrogeneration of hydrogen peroxide in acidic medium using gas diffusion electrodes modified with cobalt (II) phthalocyanine, Electrochim. Acta 104 (2013) 12–18, https://doi.org/10.1016/j.electacta.2013.04.079.
[2] K. Dong, Y. Lei, H. Zhao, J. Liang, P. Ding, Q. Liu, Z. Xu, S. Lu, Q. Li, X. Sun, Noble-metal-free electrocatalysts toward H_2O_2 production, J. Mater. Chem. A 8 (2020) 23123–23141, https://doi.org/10.1039/D0TA08894C.
[3] K. Jiang, S. Back, A.J. Akey, C. Xia, Y. Hu, W. Liang, D. Schaak, E. Stavitski, J. K. Nørskov, S. Siahrostami, H. Wang, Highly selective oxygen reduction to hydrogen peroxide on transition metal single atom coordination, Nat. Commun. 10 (2019) 3997, https://doi.org/10.1038/s41467-019-11992-2.
[4] K. Jiang, J. Zhao, H. Wang, Catalyst design for electrochemical oxygen reduction toward hydrogen peroxide, Adv. Funct. Mater. 30 (2020), 2003321, https://doi.org/10.1002/adfm.202003321.
[5] J.K. Edwards, B. Solsona, E.N. N, A.F. Carley, A.A. Herzing, C.J. Kiely, G. J. Hutchings, Switching off hydrogen peroxide hydrogenation in the direct synthesis process, Science 323 (2009) 1037–1041, https://doi.org/10.1126/science.1168980.
[6] R. Burch, P.R. Ellis, An investigation of alternative catalytic approaches for the direct synthesis of hydrogen peroxide from hydrogen and oxygen, Appl. Catal. B: Environ. 42 (2003) 203–211, https://doi.org/10.1016/S0926-3373(02)00232-1.
[7] Y. Jiang, P. Ni, C. Chen, Y. Lu, P. Yang, B. Kong, A. Fisher, X. Wang, Selective electrochemical H_2O_2 production through two-electron oxygen electrochemistry, Adv. Funct. Mater. 8 (2018), 1801909, https://doi.org/10.1002/aenm.201801909.
[8] Z. Lu, G. Chen, S. Siahrostami, Z. Chen, K. Liu, J. Xie, L. Liao, T. Wu, D. Lin, Y. Liu, T.F. Jaramillo, J.K. Nørskov, Y. Cui, High-efficiency oxygen reduction to hydrogen peroxide catalysed by oxidized carbon materials, Nat. Catal. 1 (2018) 156–162, https://doi.org/10.1038/s41929-017-0017-x.
[9] J. Zhang, G. Zhang, S. Jin, Y. Zhou, Q. Ji, H. Lan, H. Liu, J. Qu, Graphitic N in nitrogen-Doped carbon promotes hydrogen peroxide synthesis from electrocatalytic oxygen reduction, Carbon 163 (2020) 154–161, https://doi.org/10.1016/j.carbon.2020.02.084.
[10] G. Xia, Y. Tian, X. Yin, W. Yuan, X. Wu, Z. Yang, G. Yu, Y. Wang, M. Wu, Maximizing electrochemical hydrogen peroxide production from oxygen reduction with superaerophilic electrodes, Appl. Catal. B: Environ. 299 (2021), 120655, https://doi.org/10.1016/j.apcatb.2021.120655.
[11] S. Međedović, B.R. Locke, Platinum catalysed decomposition of hydrogen peroxide in aqueous-phase pulsed corona electrical discharge, Appl. Catal. B: Environ. 67 (2006) 149–159, https://doi.org/10.1016/j.apcatb.2006.05.001.
[12] E. Pizzutilo, S.J. Freakley, S. Cherevko, S. Venkatesan, G.J. Hutchings, C. H. Liebscher, G. Dehm, K.J.J. Mayrhofer, Gold–palladium bimetallic catalyst stability: consequences for hydrogen peroxide selectivity, ACS Catal. 7 (2017) 5699–5705, https://doi.org/10.1021/acscatal.7b01447.
[13] S. Siahrostami, A. Verdaguer-Casadevall, M. Karamad, D. Deiana, P. Malacrida, B. Wickman, M. Escudero-Escribano, E.A. Paoli, R. Frydendal, T.W. Hansen, I. Chorkendorff, I.E.L. Stephens, J. Rossmeisl, Enabling direct H_2O_2 production through rational electrocatalyst design, Nat. Mater. 12 (2013) 1137–1143, https://doi.org/10.1038/nmat3795.

[14] Z. Zheng, Y.H. Ng, D.-W. Wang, R. Amal, Epitaxial growth of Au–Pt–Ni nanorods for direct high selectivity H_2O_2 production, Adv. Mater. 28 (2016) 9949–9955, https://doi.org/10.1002/adma.201603662.
[15] D. Deiana, A. Verdaguer-Casadevall, P. Malacrida, I.E.L. Stephens, I. Chorkendorff, J.B. Wagner, T.W. Hansen, Determination of core–shell structures in Pd-Hg nanoparticles by STEM-EDX, ChemCatChem 7 (2015) 3748–3752, https://doi.org/10.1002/cctc.201500791.
[16] C. Xia, J.Y. Kim, H. Wang, Recommended practice to report selectivity in electrochemical synthesis of H_2O_2, Nat. Catal. 3 (2020) 605–607, https://doi.org/10.1038/s41929-020-0486-1.
[17] Y. Sun, L. Silvioli, N.R. Sahraie, W. Ju, J. Li, A. Zitolo, S. Li, A. Bagger, L. Arnarson, X. Wang, T. Moeller, D. Bernsmeier, J. Rossmeisl, F. Jaouen, P. Strasser, Activity–selectivity trends in the electrochemical production of hydrogen peroxide over single-site metal–nitrogen–carbon catalysts, J. Am. Chem. Soc. 141 (2019) 12372–12381, https://doi.org/10.1021/jacs.9b05576.
[18] C. Tang, L. Chen, H. Li, L. Li, Y. Jiao, Y. Zheng, H. Xu, K. Davey, S.-Z. Qiao, Tailoring acidic oxygen reduction selectivity on single-atom catalysts via modification of first and second coordination spheres, J. Am. Chem. Soc. 743 (2021) 7819–7827, https://doi.org/10.1021/jacs.1c03135.
[19] L. Ai, C. Zhang, L. Li, J. Jiang, Iron terephthalate metal–organic framework: revealing the effective activation of hydrogen peroxide for the degradation of organic dye under visible light irradiation, Appl. Catal. B: Environ., 148- 149 (2014) 191–200, https://doi.org/10.1016/j.apcatb.2013.10.056.
[20] Y. Ding, W. Zhou, J. Gao, F. Sun, G. Zhao, H_2O_2 electrogeneration from O_2 electroreduction by N-Doped carbon materials: a mini-review on preparation methods, selectivity of N sites, and prospects, Adv. Mater. Interfaces 8 (2021), 2002091, https://doi.org/10.1002/admi.202002091.
[21] Q. Li, Y. Chen, F. Du, X. Cui, L. Dai, Bias-free synthesis of hydrogen peroxide from photo-driven oxygen reduction reaction using N-doped γ-graphyne catalyst, Appl. Catal. B: Environ. 304 (2022), 120959, https://doi.org/10.1016/j.apcatb.2021.120959.
[22] Y. Xia, X. Zhao, C. Xia, Z.-Y. Wu, P. Zhu, J.Y. Kim, X. Bai, G. Gao, Y. Hu, J. Zhong, Y. Liu, H. Wang, Highly active and selective oxygen reduction to H_2O_2 on boron-doped carbon for high production rates, Nat. Commun. 12 (2021) 4225, https://doi.org/10.1038/s41467-021-24329-9.
[23] F. Ma, S. Wang, X. Liang, C. Wang, F. Tong, Z. Wang, P. Wang, Y. Liu, Y. Dai, Z. Zheng, B. Huang, Ni_3B as a highly efficient and selective catalyst for the electrosynthesis of hydrogen peroxide, Appl. Catal. B: Environ. 279 (2020), 119371, https://doi.org/10.1016/j.apcatb.2020.119371.
[24] V. Perazzolo, C. Durante, R. Pilot, A. Paduano, J. Zheng, G.A. Rizzi, A. Martucci, G. Granozzi, A. Gennaro, Nitrogen and sulfur doped mesoporous carbon as metal-free electrocatalysts for the in situ production of hydrogen peroxide, Carbon 95 (2015) 949–963, https://doi.org/10.1016/j.carbon.2015.09.002.
[25] H. Zhang, X. Bai, Photocatalytic production of hydrogen peroxide over Z-scheme Mn_3O_4/Co_9S_8 with p-n heterostructure, Appl. Catal. B: Environ. 298 (2021), 120516, https://doi.org/10.1016/j.apcatb.2021.120516.
[26] B.-Q. Li, C.-X. Zhao, J.-N. Liu, Q. Zhang, Electrosynthesis of Hydrogen Peroxide Synergistically Catalyzed by Atomic Co–Nx–C Sites and Oxygen Functional Groups in Noble-Metal-Free Electrocatalysts, Adv. Mater. 31 (2019), 1808173, https://doi.org/10.1002/adma.201808173.
[27] Q. Zhao, N. Li, C. Liao, L. Tian, J. An, X. Wang, The UV/H_2O_2 process based on H_2O_2 in-situ generation for water disinfection, J. Hazard. Mater. Lett. 2 (2021), 100020, https://doi.org/10.1016/j.hazl.2021.100020.
[28] C. Zhang, W. Liu, M. Song, J. Zhang, F. He, J. Wang, M. Xiong, J. Zhang, D. Wang, Pyranoid-O-dominated graphene-like nanocarbon for two-electron oxygen reduction reaction, Appl. Catal. B: Environ. 307 (2022), 121173, https://doi.org/10.1016/j.apcatb.2022.121173.
[29] K. Zhao, Y. Su, X. Quan, Y. Liu, S. Chen, H. Yu, Enhanced H_2O_2 production by selective electrochemical reduction of O_2 on fluorine-doped hierarchically porous carbon, J. Catal. 357 (2018) 118–126, https://doi.org/10.1016/j.jcat.2017.11.008.
[30] X. Yan, D. Li, L. Zhang, X. Long, D. Yang, Tuning oxygen-containing groups of pyrene for high hydrogen peroxide production selectivity, Appl. Catal. B: Environ. 304 (2022), 120908, https://doi.org/10.1016/j.apcatb.2021.120908.
[31] X.X. Wang, V. Prabhakaran, Y. He, Y. Shao, G. Wu, Iron-free cathode catalysts for proton-exchange-membrane fuel cells: cobalt catalysts and the peroxide mitigation approach, Adv. Mater. 31 (2019), 1805126, https://doi.org/10.1002/adma.201805126.
[32] W. Liu, C. Zhang, J. Zhang, X. Huang, M. Song, J. Li, F. He, H. Yang, J. Zhang, D. Wang, Tuning the atomic configuration of Co-N-C electrocatalyst enables highly-selective H2O2 production in acidic media, Appl. Catal. B: Environ. 310 (2022), 121312, https://doi.org/10.1016/j.apcatb.2022.121312.
[33] G. Zhong, D. Liu, J. Zhang, The application of ZIF-67 and its derivatives: adsorption, separation, electrochemistry and catalysts, J. Mater. Chem. A 6 (2018) 1887–1899, https://doi.org/10.1039/C7TA08268A.
[34] T. Wang, C. Yang, Y. Liu, M. Yang, X. Li, Y. He, H. Li, H. Chen, Z.J.Nl Lin, Dual-Shelled multidoped hollow carbon nanocages with hierarchical porosity for high-performance oxygen reduction reaction in both alkaline and acidic media, Nano Lett. 20 (2020) 5639–5645, https://doi.org/10.1021/acs.nanolett.0c00081.
[35] V. Nallathambi, J.-W. Lee, S.P. Kumaraguru, G. Wu, B.N. Popov, Development of high performance carbon composite catalyst for oxygen reduction reaction in PEM proton exchange membrane fuel cells, J. Power Sources 183 (2008) 34–42, https://doi.org/10.1016/j.jpowsour.2008.05.020.
[36] Y. Song, D. Sun, X. Jiang, H. Ma, C. Ma, J. Hao, X. Zhang, Enhanced activation of peroxymonosulfate by bimetallic spinel sulfides $CoNi_2S_4$ for organic dye degradation, J. Environ. Chem. Eng. 9 (2021), 106889, https://doi.org/10.1016/j.jece.2021.106889.
[37] Y. Sun, I. Sinev, W. Ju, A. Bergmann, S. Dresp, S. Kühl, C. Spöri, H. Schmies, H. Wang, D. Bernsmeier, B. Paul, R. Schmack, R. Kraehnert, B. Roldan Cuenya, P. Strasser, Efficient electrochemical hydrogen peroxide production from molecular oxygen on nitrogen-doped mesoporous carbon catalysts, ACS Catal. 8 (2018) 2844–2856, https://doi.org/10.1021/acscatal.7b03464.
[38] J. Gao, Hb Yang, X. Huang, S.-F. Hung, W. Cai, C. Jia, S. Miao, H.M. Chen, X. Yang, Y. Huang, T. Zhang, B. Liu, Enabling direct H_2O_2 production in acidic media through rational design of transition metal single atom catalyst, Chem 6 (2020) 658–674, https://doi.org/10.1016/j.chempr.2019.12.008.
[39] E. dJung, H. Shin, B.-H. Lee, V. Efremov, S. Lee, H.S. Lee, J. Kim, W. Hooch Antink, S. Park, K.-S. Lee, S.-P. Cho, J.S. Yoo, Y.-E. Sung, T. Hyeon, Atomic-level tuning of Co–N–C catalyst for high-performance electrochemical H_2O_2 production, Nat. Mater. 19 (2020) 436–442, https://doi.org/10.1038/s41563-019-0571-5.
[40] T. Murayama, I. Yamanaka, Electrosynthesis of neutral H_2O_2 solution from O_2 and water at a mixed carbon cathode using an exposed solid-polymer-electrolyte electrolysis cell, J. Phys. Chem. C. 115 (2011) 5792–5799, https://doi.org/10.1021/jp1109702.
[41] Y. Zhu, R. Zhu, Y. Xi, T. Xu, L. Yan, J. Zhu, G. Zhu, H. He, Heterogeneous photo-Fenton degradation of bisphenol A over Ag/AgCl/ferrihydrite catalysts under visible light, Chem. Eng. J. 346 (2018) 567–577, https://doi.org/10.1016/j.cej.2018.04.073.
[42] K. Wang, K. Zhao, X. Qin, S. Chen, H. Yu, X. Quan, Treatment of organic wastewater by a synergic electrocatalysis process with Ti^{3+} self-doped TiO_2 nanotube arrays electrode as both cathode and anode, J. Hazard. Mater. 424 (2022), 127747, https://doi.org/10.1016/j.jhazmat.2021.127747.